Plasma Phys. Control. Fusion **40** (1998) 1127–1147. Printed in the UK PII: S0741-3335(98)85947-2

Helical post stellarator

Paul E Moroz

Center for Plasma Theory and Computation, Department of Engineering Physics, University of Wisconsin, Madison, WI 53706, USA

Received 14 July 1997, in final form 19 January 1998

Abstract. A novel type of stellarator device, the helical post stellarator (HPS), is introduced. Calculations are given for a particular HPS configuration, the single-helix stellarator (SHS) featuring a single-helix centre post. This configuration is significantly different from all previously known stellarators due to the combination of its unique geometrical characteristics and physical properties. Among these are the facts that the helical magnetic field has only one toroidal period ($N = 1$), the plasma has an extremely low aspect ratio, $A \approx 1$, and the variation of the magnetic field, B, along field lines features a helical ripple entirely on the inside of the torus. Among the main advantages of an HPS for the fusion program are an extremely compact, modular, and simple design compatible with significant rotational transform, large plasma volume, and improved particle transport characteristics.

1. Introduction

Traditionally, stellarators are large-aspect-ratio machines with an aspect ratio A (which is the ratio of the average major radius, R, to the average minor radius, a, for the last closed flux surface) of around 10. The so-called low-A stellarators [1] have aspect ratios $A \approx 5$–7. The lowest-A stellarators ever built are the Compact Helical System (CHS) [2], the Compact Auburn Torsatron (CAT) [3], and the heliac H-1 [4], which have $A \approx 5$. Record values of the volume average $\beta \approx 2.1\%$ in stellarators have been reported [2] for the low-A stellarator CHS (although the highest β values reached in the large-A stellarators come close to this result: $\beta \leqslant 1.8\%$ in W7-AS [5] and $\beta \leqslant 2\%$ in Heliotron-E [6]).

In parallel to the development of the world spherical tokamak (ST) program [7–14], which promises more compact, higher β, and a less disruptive approach for tokamaks, the spherical stellarator (SS) program has been initiated recently [15–22] for machines with stellarator features and the aspect ratio A below 3.5. The plasma current enhancing the vacuum rotational transform is one of the key elements of the SS approach. The SS concept offers a significantly different (from traditional stellarator or tokamak approaches) way to a fusion reactor, which can be envisioned as a compact and inexpensive machine with the steady-state, high-β, and strong bootstrap current regimes of operation and good particle confinement. From this point of view, a few simple and fundamentally different SS configurations have recently been investigated: with a straight centre post [15, 16], with planar coils [17, 18], and with outboard stellarator windings [19]. Various combinations of these main types can result in a more general modular twisted coil approach [21, 22] and might correspond to parameter optimization. For the SS considered, it was shown [15–22] that a positive plasma current via inductive drive or the bootstrap effect is advantageous for reaching higher β equilibria and improved transport characteristics.

0741-3335/98/061127+21$19.50

In our search for the optimal SS configuration, we do not impose any special limitations (and have not included them in a definition of the SS concept) on how to reach the improved confinement in an SS, because we are checking various possibilities and trying to simultaneously satisfy not only the requirement of improved confinement but also that of high-β regimes of operation, an efficient coil system and a divertor, simplicity, modularity and compactness of the configuration etc, which can open a better path to a fusion reactor.

More recently, however, a few other US institutions have become involved in SS-type research. They decided to focus their investigations on a particular way of reaching the improved confinement. Researchers at ORNL focus on J^* transport optimization, and they have used the name SMARTH (SMall Aspect Ratio Toroidal Hybrid) for a device [21–26]. A different case of SS optimization regarding the particle transport can be based on a quasi-axisymmetric approach. The natural tendency of the magnetic structure in an SS to become more quasi-axisymmetric with increasing plasma current has been stressed in [20, 21]. Stellarator coil systems especially designed for obtaining vacuum magnetic field configurations with quasi-axisymmetric properties have been discussed in recent publications [27–29]. There, such configurations were called the Modular Helias-like Heliac 2 (MHH2). In those publications, the author reduced the plasma aspect ratio first to $A = 4.5$ [27], then to $A = 3.5$ [28], and lastly to $A = 3.2$ [29], thus moving gradually into the SS domain regarding the plasma aspect ratio, although without including the plasma current. More recently, the PPPL team [30–32] started to use this quasi-axisymmetric approach for transport optimization in SS-type devices with the plasma current. The aspect ratios for the magnetic field configurations presently being considered by the ORNL and PPPL teams are $A \approx 2.5$–3.5.

The present paper introduces a new family of SS-type configurations called the helical post stellarators (HPS). Moreover, this paper is devoted to a particular HPS configuration, the single-helix stellarator (SHS), which features a single-helix centre post. In the following it is shown that an SHS features (together with some other advantages) improved particle transport. This demonstrates that there is at least one more path (it can be called, as will become clear from the discussion, a 'generalized σ-optimization') to improved confinement in an SS, apart from quasi-axisymmetry or J^* optimization. Simultaneous satisfaction (to some degree) of all these three different optimization principles might give better results than a closer satisfaction to only one such principle.

An SHS configuration is unique in comparison with traditional stellarator devices (even compared with the SS systems considered so far) and sets a few records for stellarators. First, an SHS is a stellarator configuration with a single toroidal period ($N = 1$). To our knowledge, there have only been two other stellarator configurations with $N = 1$ proposed and briefly discussed: the Cleftron [33] and the Ultra-Simple Stellarator [34]. Both of these configurations had straight centre columns. The Cleftron's coil system consists of a single outboard helical winding connecting the bottom and top parts of the straight centre column and making one turn around it, while the Ultra-Simple Stellarator has two interconnected planar coils: a small circular and a very large rectangular. These $N = 1$ configurations, however, do not feature many attractive characteristics of the SHS.

The HPS configurations differ from any other stellarator in that they do not have the traditional stellarator helical windings or twisted coils encircling the plasma, and their only (or main) helical element is a helical post located in the centre of the torus. The plasma aspect ratios, $A \approx 1$–1.5, obtained in the HPS configurations are also out of the range considered for stellarators. (In fact, in this paper, we discuss the configurations with plasma aspect ratios in the range 1–1.25. The higher A were obtained, however, for other HPS configurations briefly mentioned in the last paragraph of the paper). A relatively large

rotational transform, $\iota \approx 0.1$–0.15, found for these extremely low aspect ratios, and the inboardly located helical ripple (which means improved particle transport [35, 36]) represent the significant advantages of these configurations. Taking into account all these factors together with the extreme simplicity of the coil system makes an SHS of particular interest for fusion applications.

The neoclassical transport theory in stellarators was developed first [37, 38] for a simple magnetic field model,

$$B/B_0 = 1 - \varepsilon_t \cos\theta - \varepsilon_h \cos\eta \tag{1}$$

where B_0 is the central magnetic field, $\eta = m\theta - nN\varphi$, m and n are the poloidal and toroidal mode numbers, N is the number of toroidal field periods, and θ and φ are the poloidal and toroidal angles. This model field includes just the main toroidal and helical harmonics caused by the toroidicity and helical windings. The theory predicts significant particle and energy fluxes in the low collisionality $1/\nu$ regime, which are proportional to $\varepsilon_t^2 \varepsilon_h^{3/2}/\nu$, with ν being the collision frequency. However, real stellarators usually have a significantly more complicated spectrum of helical harmonics than that given by equation (1). As was first found numerically via the Monte Carlo simulations [39], additional helical harmonics can significantly improve the transport characteristics of a stellarator to the extend that the dangerous $1/\nu$ regime is absent. The theoretical analysis and Monte Carlo calculations of [35] explained this effect by considering a more complicated model field,

$$B = B_0[1 - \varepsilon_t \cos\theta - \varepsilon_h \cos\eta(1 - \sigma\cos\theta)] \tag{2}$$

which is different from (1) in the case of non-zero σ. It was found that for $\sigma \approx \varepsilon_h/\varepsilon_t \approx 1$ the radial drift of the helically trapped particles is reduced significantly, and a numerical example has demonstrated the reduction of neoclassical diffusion by an order of magnitude in comparison with the case of $\sigma = 0$ and the same ε_t and ε_h. Later theory and numerical calculations [36, 40] generalized and confirmed these results for configurations with multiple harmonics. The main conclusion was the same—an order of magnitude reduction of neoclassical transport coefficients is possible if the helical ripple is localized inboard of the torus.

For low-aspect-ratio stellarators in general, and especially for the SS configurations where both ε_t and ε_h are significant, neoclassical transport can be, in principle, very large and requires careful optimization. Taking into account the above mentioned facts, we searched for an SS configuration that had an inboardly located magnetic ripple. The SHS system, discussed below, gives a simple, interesting and unusual example of such a configuration.

The rest of this paper is organized as follows. In section 2, the coil system of an SHS is described. In section 3, the main parameters of the vacuum magnetic field configuration without poloidal field (PF) rings are given, and section 4 demonstrates similar results for a configuration with PF rings. The effects of plasma current are discussed in section 5. The results of calculations of the S-factor and neoclassical transport are presented in section 6. Finally, the main conclusions are summarized in section 7.

2. The coil system of an SHS

The HPS coil configuration can be obtained from a typical ST coil system [7] by replacing the straight centre post of an ST with the helical post, as shown in figure 1 for an SHS. The outboard parts of TF coils can be the same as in an ST and can feature remote (or a large number of) return conductors to reduce the outboard magnetic field ripple. Consequently, the total current of all TF coils goes through a single helical centre post (HCP), or equivalently,

through the number of close conductors of an HCP. Similar to modifying an ST, the HPS can be obtained by replacing the straight centre post of an SS configuration of [15, 16] with the HCP. In this paper, however, we will consider only the first option (modification of an ST), while the second option (modification of an SS) will be discussed elsewhere.

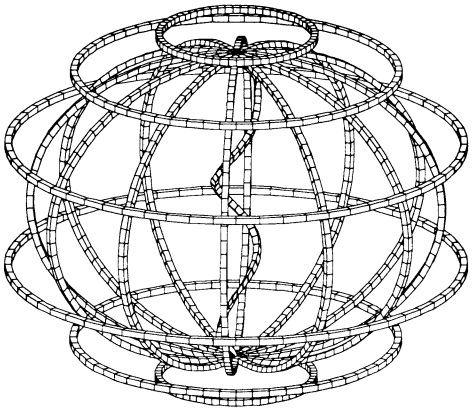

Figure 1. An SHS coil system.

The configuration presented in figure 1 corresponds to the first round of the coil system optimization regarding the extreme low aspect ratio, large enclosed volume, large vacuum rotational transform, small outboard magnetic field ripple, and small magnetic island structure. The coil system shown includes 12 outboard (half-elliptical) TF coils, three pairs of PF rings, and a single HCP making 1.5 turns around the vertical axis ($\Delta\varphi_{cp} = 3\pi$). The winding law for the HCP presented in the figures in this paper was chosen as

$$\varphi = \frac{\Delta\varphi_{cp}}{2}\sin\left(\frac{\pi z}{2H}\right) \qquad R = R_{cp}(1-\zeta^2)^2 \tag{3}$$

where φ is the toroidal angle, z is the distance from the equatorial plane, R is the distance from the vertical axis (major radius), H is the half-height of the HCP, and the parameter $\zeta = 0$ for $|z| \leqslant h$, and $\zeta = (|z|-h)/(H-h)$ for $h < |z| \leqslant H$, with h being the half-length of the central part of the HCP. The dimensions chosen for an example of a system with good parameters are: $R_{cp} = 0.1$ m, $h = 0.6$ m, and $H = 0.75$ m.

A set of three pairs of PF rings, shown in figure 1, is not a necessary element for forming the vacuum flux surfaces. It is, however, advantageous for shaping the flux surfaces, optimizing the magnetic ripple, adjusting the plasma aspect ratio, and controlling the plasma location. It will be useful also for reaching high β in the regimes with the finite plasma pressure and finite plasma current.

3. The SHS configuration without PF rings

Tracing along field lines, carried out via the UBFIELD code (see, for example, [41]) for the coil configuration and parameters discussed in the previous section, demonstrates a number of peculiar characteristics of the SHS magnetic field. First we discuss the configuration without PF rings.

The closed vacuum flux surfaces of large volume are shown in figures 2 and 3 for two perpendicular cross sections of the device, respectively in the X–Z and Y–Z planes of the Cartesian coordinate system with Z being the vertical axis, and the X–Z plane corresponding

to $\varphi = 0$ and $\varphi = \pi$. The cross sections of outboard parts of the TF coils and the HCP are also presented in these figures. The Poincaré puncture plots calculated for a large number of closed flux surfaces demonstrate that the enclosed area is practically island-free, although the narrow chains of magnetic islands are present for flux surfaces where the rotational transform, ι, goes through rational values, such as 1/9, 1/10, 1/11, etc. These resonances can be enhanced if the corresponding helical harmonics with $n = 1$ and $m = 9$, 10, 11 etc have significant amplitudes in the spectrum of the magnetic field for the corresponding flux surfaces. Here, n and m are the toroidal and poloidal mode numbers, respectively. It is not a problem, however, for the SHS, at least not for the vacuum configuration considered. One can see that the magnetic islands are too narrow to affect the plasma confinement in the SHS. However, finite-β calculations for magnetic islands should be carried out before an actual high-β experiment is designed. The aspect ratio of the configuration presented is extremely low, $A = 1.17$, which has never been considered before for stellarators.

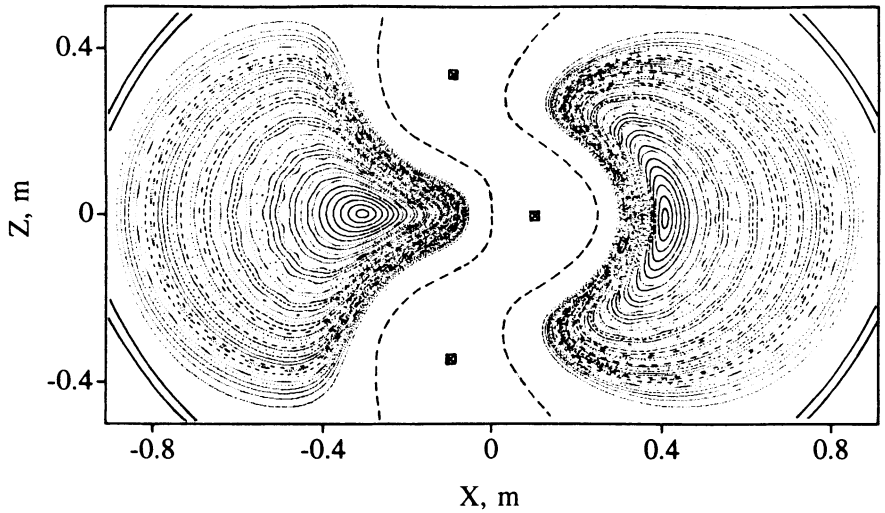

Figure 2. Poincaré puncture plots for closed vacuum flux surfaces in the X–Z cross section. The dashed curves demonstrate the geometry of the open field lines. Cross sections of the coils are also shown.

The dashed curves in figures 2 and 3 demonstrate the geometry of the opened field lines. These field lines go along the HCP and might serve as part of the divertor system with the divertor plates conveniently located at the top and bottom parts of an SHS where some free space is readily available (see figure 4, which shows schematically the whole coil configuration together with the three main plasma cross sections).

The perspective view of the coil system and the last closed vacuum flux surface is given in figure 5. One can see the periodic modulation induced by the 12 TF coils and that the last flux surface extends further into the space between the TF coils. This effect is similar to that in a tokamak or in any other toroidal configuration with a finite number of TF coils, and is caused by the proximity of the flux surface to the TF coils. The corresponding outboard magnetic ripple (see figure 6(a) for the last closed flux surface, $\rho = 1$, where ρ is the normalized average minor radius) might increase the transport coefficients significantly and thus should be avoided. The full black regions in figure 6(a) are the high spatial frequency TF ripple. This ripple is reduced significantly for the internal flux surfaces, and figure 6(b)

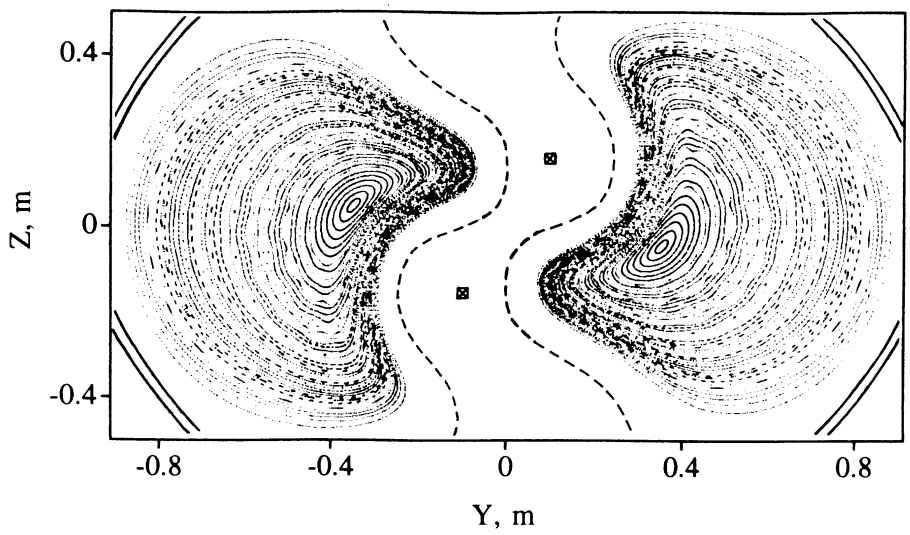

Figure 3. Same as figure 2, but for the $Y-Z$ cross section.

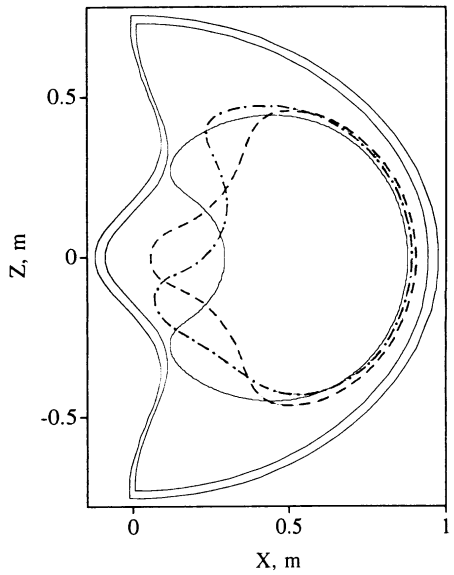

Figure 4. A poloidal projection of the SHS coil system together with the main cross sections of the last closed flux surface.

demonstrates, as an example, that it is practically absent for a flux surface with $\rho = 0.5$. The same 12-period modulation can be seen in figure 7(a) showing the $|B|$ distribution on the flux surface, $\rho = 1$. There, B_0 designates the value of the first full contour, and ΔB is the difference between adjacent contour lines. Full contours correspond to $|B| \geqslant B_0$, while the dotted contours correspond to $|B| < B_0$. The $|B|$ bumpiness is not seen for the flux surface $\rho = 0.5$ (figure 7(b)), where the helical symmetry of $|B|$ on the inboard changes to toroidal symmetry on the outboard of the flux surface. A few methods can be used to reduce

the outboard ripple, which are mainly based either on moving the plasma further from the outboard parts of the TF coils or on increasing their number. To accomplish the former, additional divertor coils or limiters can be used, or the vertical magnetic field produced by PF rings can be applied to move the plasma closer to the centre.

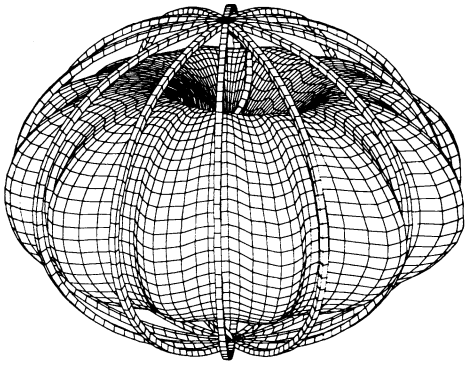

Figure 5. A perspective view of the SHS plasma and the coils.

The equatorial ($Z = 0$) cross section of the plasma is given in figure 8 where cross sections for TF coils and for the HCP are also presented. The magnetic axis projection is shown by the dashed curve, which seems to be circular although it is non-planar in reality. The helical space around the HCP is free of plasma and naturally prevents the HCP conductors from contacts with the hot plasma. In the calculations of the magnetic field, presented in figures 6 and 7, the total current through the HCP was $I_{cp} = 600$ kA which allowed us to obtain a magnetic field at the plasma centre of about 1 T. This fact demonstrates the high efficiency of the SHS coil system which is capable of producing high magnetic fields in the plasma region with moderate currents in the coils.

The radial dependence of the rotational transform, $\iota = 1/q$ (q being the safety factor), is shown in figure 9 (full curve) and it varies from 0.123 at the axis to 0.055 at the plasma edge. From the point of view of advanced large-aspect-ratio stellarators, which often have $\iota \sim 1$, such a rotational transform is small. However, for the extreme-low-aspect-ratio machine considered, it is large. One has to compare not the ι values themselves but rather the ι/A values, which is really the ratio of the average minor plasma radius to the connection length. These values are not smaller for this SHS when compared to traditional or advanced stellarators. In fact, these values of ι, found for the SHS without any plasma current, are only a factor of two or three lower than that considered for stable regimes in spherical tokamaks with large plasma current [13]. The vacuum ι represents a significant contribution to the total rotational transform of an SHS in its more optimal regimes of operation with the plasma current (see section 5) and can serve (at high β) as a seed for the bootstrap current [15, 16, 21].

4. The SHS configuration with PF rings

As was mentioned above, the PF rings should be retained as an important element of the HPS coil system to control both the vacuum magnetic field configuration and the configuration at finite plasma pressure and finite plasma current. Here we show that small currents in PF rings (about 4 kA each, which is small in comparison with $I_{cp} = 600$ kA) can be used

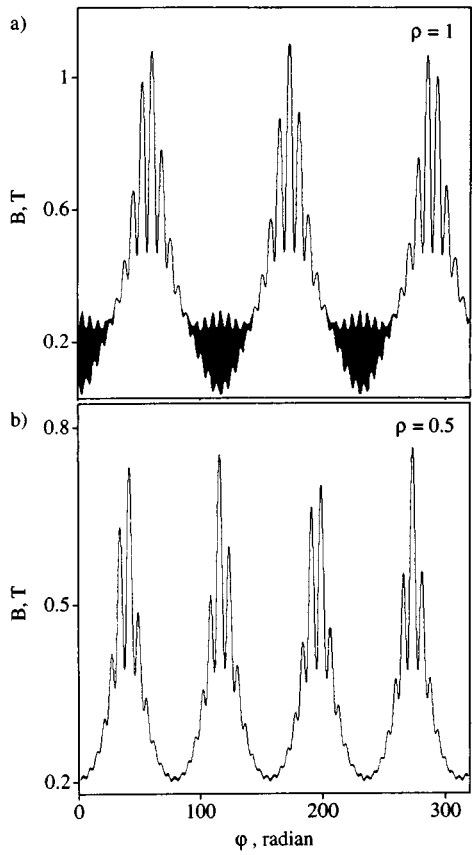

Figure 6. Magnetic field variation along a field line: (a) for the last flux surface, $\rho = 1$; (b) for the flux surface, $\rho = 0.5$.

effectively to reduce the outboard magnetic ripple and control the aspect ratio of the vacuum magnetic configuration.

The location of the PF rings in this example can be seen in figure 10, where the TF coil and the HCP projections are also drawn and the main cross sections of the last closed vacuum flux surface are shown. In this case, the plasma is shifted inboard and is more vertically elongated. The plasma aspect ratio is $A = 1.02$. The corresponding perspective view of the coil system and the last closed flux surface is given in figure 11, which demonstrates rather well a near spherical-shaped plasma of the SHS with a modest central opening through which the HCP extends. The puncture tracings of the large number of closed flux surfaces is given in figure 12 (for the X–Z cross section) and figure 13 (for the Y–Z cross section). They demonstrates clearly the absence of significant magnetic islands in the SHS configuration considered.

The radial dependence of the rotational transform is shown in figure 9 by the dashed curve. It varies from $\iota(0) = 0.15$ to $\iota(1) = 0.045$ and for most of the plasma volume it is larger than that for the case without PF rings.

Magnetic field variation along the field line, for the last closed flux surface, is shown in figure 14(a). Because the plasma for this case is pushed inward, the magnetic field magnitude increases and reaches $B_{\max} = 1.7$ T for the same current in the centre post of 600 kA. Thus,

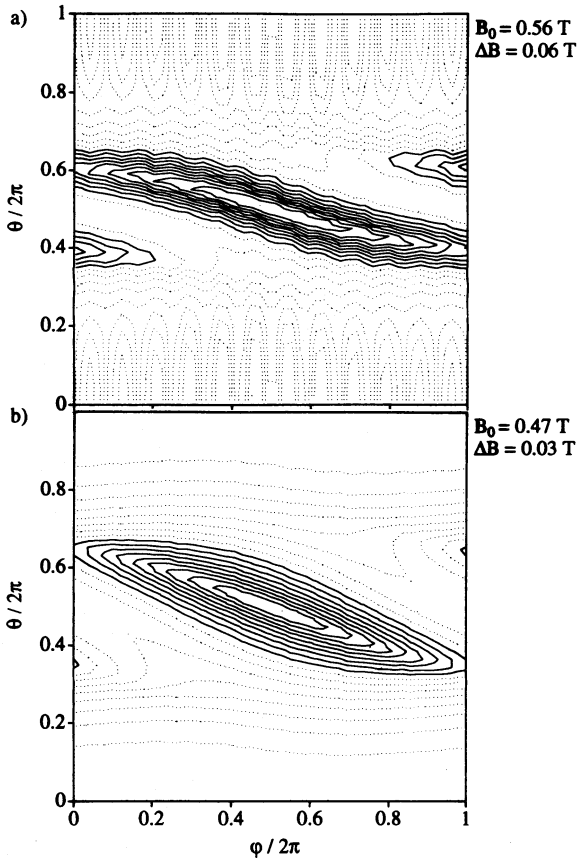

Figure 7. (a) The distribution of $|B|$ on flux surfaces: (a) flux surface $\rho = 1$; (b) $\rho = 0.5$. B_0 corresponds to the value of the first full contour, and ΔB is the difference between the adjacent contours. Full contours correspond to $|B| \geqslant B_0$, and dotted contours to $|B| < B_0$.

the efficiency of the coils in producing high magnetic fields in the plasma region is even higher. The outboard magnetic ripple is also significantly reduced. Further reduction of the outboard ripple (practically, its total elimination) can be obtained by increasing the number of TF coils to $N_c = 24$ (figure 14(b)).

5. The SHS configuration with plasma current

Analysis of a few different SS-type configurations [15–22] has stressed the importance of a positive plasma current, externally driven or arising internally via the bootstrap effect. Positive current means that it flows in the direction to increase the total rotational transform in comparison with its vacuum value. A requirement for this type of plasma current was even included among the four defining characteristics of the SS concept [15–22] (the other three were concerned with the low aspect ratio, the high-β regimes, and good confinement).

In this section we give an example of the SHS configuration with plasma current. The moderate plasma current of 33 kA with centrally peaked current profile (ohmic type) was chosen to be in the form $J/J_0 = (1 - \rho^2)^2$. The number of TF coils was $N_c = 24$, the

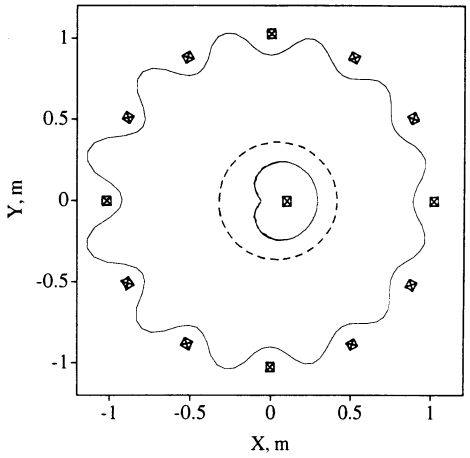

Figure 8. The equatorial cross section ($Z = 0$) of the plasma; the cross sections of the TF coils and the HCP are also presented. The magnetic axis projection is shown by the dashed curve.

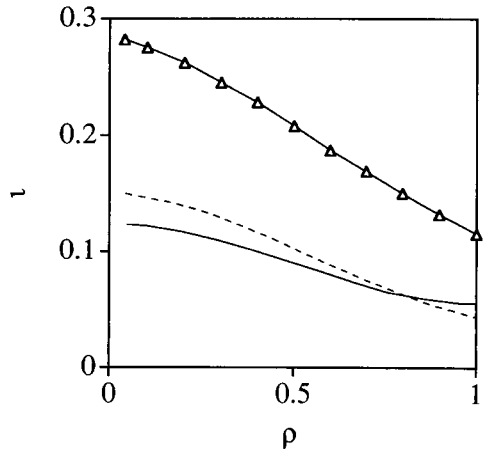

Figure 9. The radial dependence of the rotational transform for the SHS without PF rings (full curve), with PF rings (dashed curve), and with the plasma current (triangles).

PF rings were not used, and the plasma pressure was very low. Calculations were carried out via the 3D MHD equilibrium code, VMEC [42], running in free-boundary mode. This mode is of importance because the plasma boundary shape varies depending on the plasma current.

The MHD equilibrium found, with a set of nested flux surfaces, is given in figures 15(a) and (b), where the X–Z and Y–Z plasma cross sections are shown. The plasma aspect ratio, $A = 1.25$, is slightly larger than in the previously considered vacuum cases, and the total rotational transform (a curve with triangles in figure 9) is about twice its vacuum value.

One of the important effects of the plasma current on the SHS properties is a modification of the magnetic well, W, which is usually defined through the integral, $U = \int \mathrm{d}l/B$, taken along a field line and averaged over the flux surface:

$$W(\rho) = 1 - \langle U(\rho)\rangle / \langle U(0)\rangle.$$

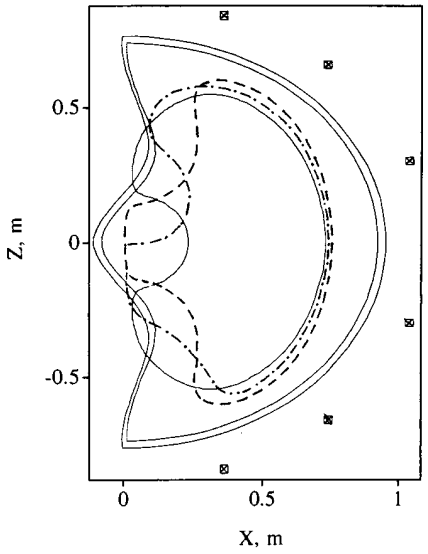

Figure 10. The poloidal projection of the SHS coil configuration with PF rings, together with the main cross sections of the last closed flux surface.

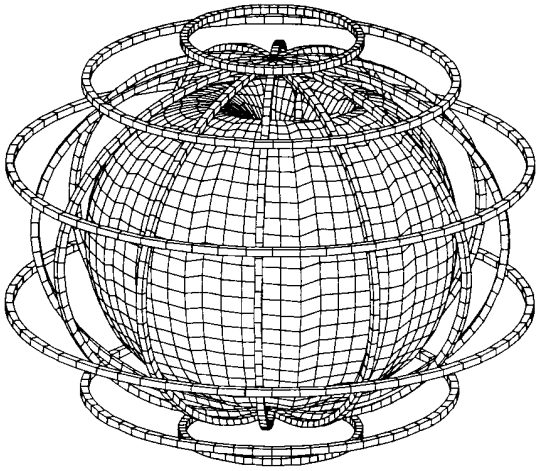

Figure 11. A perspective view of the SHS plasma and the coils corresponding to the SHS configuration with PF rings.

The vacuum SHS configurations of previous sections have featured the total magnetic hill of $W_1 = -1.5$ for the case without PF rings, and $W_2 = -0.5$ with PF rings. Although we cannot judge without the MHD stability calculations whether these values of the magnetic hill in the vacuum SHS configurations are dangerous for the stability, it is clear that making these hills into wells will only ward against possible instabilities. The plasma current produces the effect of the magnetic well and the results of calculations are shown in figure 16. In this case, the magnetic well reaches 10.3% at $\rho = 0.7$ and then decreases to 7.4% near the plasma edge. This is a rather strong magnetic well in comparison with that for a typical stellarator.

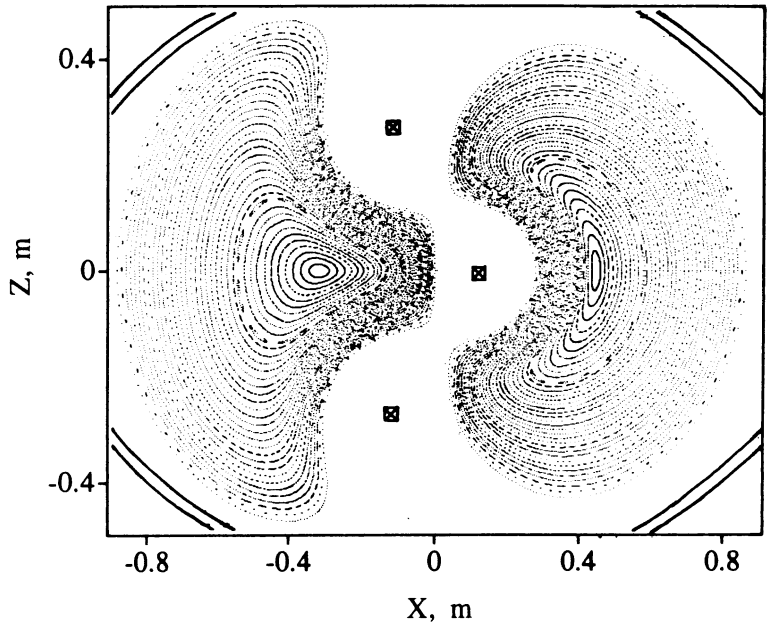

Figure 12. Poincaré puncture plots for the SHS configuration with PF rings. The X–Z cross section is shown.

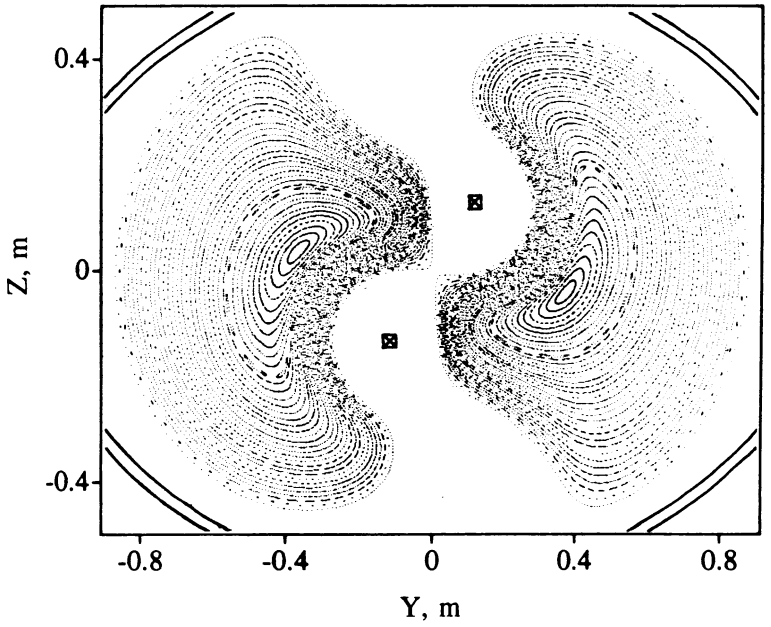

Figure 13. Same as figure 12, but for the Y–Z cross section.

The positive effects of the plasma current on particle transport in a SHS are discussed in the next section.

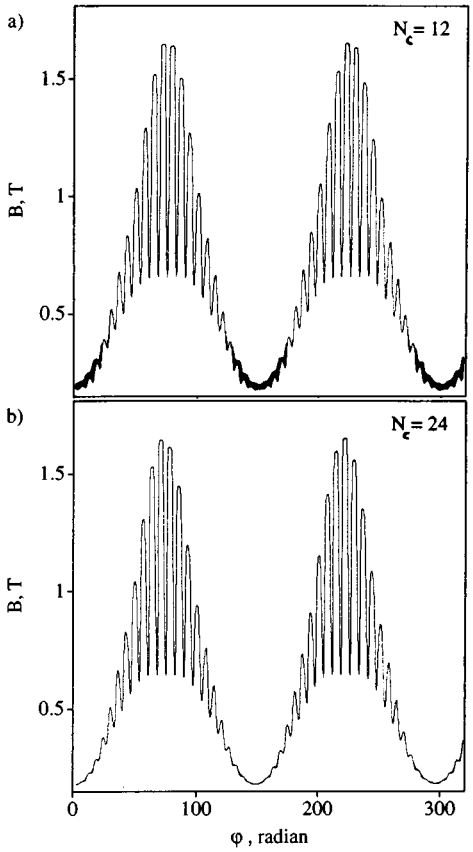

Figure 14. Magnetic field variation along a field line for the last closed vacuum flux surface in the SHS configuration with PF rings: (a) with 12 TF coils; (b) with 24 TF coils.

6. Particle transport in an SHS

Neoclassical particle and energy fluxes in stellarators (see, for example, [35, 36]) at low collisionality can be expressed through the geometrical factor, S, first considered in [36]. Let us present this factor for the general magnetic field of the form

$$B/B_0 = 1 + \sum_{mn} \varepsilon_{mn} \cos(m\theta - nN\varphi) \tag{4}$$

used in our calculations, where the index $n = 0, 1, 2$, etc, while the index m includes both negative and positive modes. This general form includes, as particular cases, the model forms given by equations (1) and (2). For those cases, $\varepsilon_{\mathrm{t}} = -\varepsilon_{10}$ and $\varepsilon_{\mathrm{h}} = -\varepsilon_{m_0,n_0}$, where m_0 and n_0 correspond to the main helical harmonic (usually, $n_0 = 1$, which also holds for the SHS configuration considered). The factor, σ, in equation (2) comes from two equal neighbouring poloidal harmonics $\varepsilon_{m_0+1,n_0} = \varepsilon_{m_0-1,n_0}$, so that $\sigma = -2\varepsilon_{m_0+1,n_0}/\varepsilon_{m_0,n_0}$. The θ and φ angles correspond to the Boozer coordinate system [43].

The parameter, S, for the general field of equation (4) can be defined as

$$S = \frac{1}{\rho^2} \int_0^{2\pi} \mathrm{d}\theta\, \varepsilon_{\mathrm{H}}^{3/2} \left[1.778 \left(\frac{\partial \varepsilon_{\mathrm{T}}}{\partial \theta} \right)^2 - 2.133 \left(\frac{\partial \varepsilon_{\mathrm{T}}}{\partial \theta} \right) \left(\frac{\partial \varepsilon_{\mathrm{H}}}{\partial \theta} \right) + 0.684 \left(\frac{\partial \varepsilon_{\mathrm{H}}}{\partial \theta} \right)^2 \right] \tag{5}$$

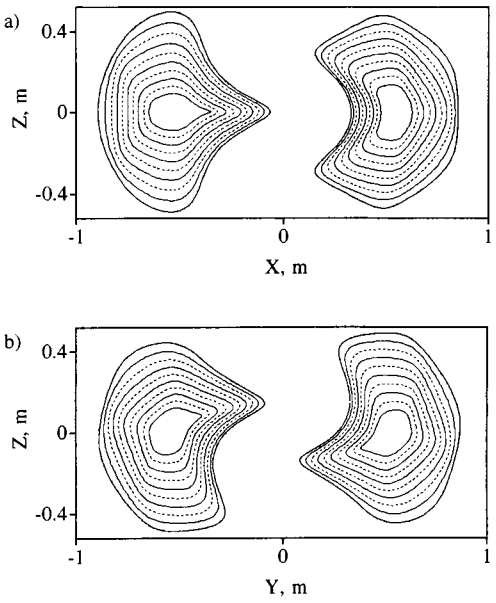

Figure 15. Flux surfaces for the MHD equilibrium in an SHS with plasma current: (a) X–Z cross section; (b) Y–Z cross section.

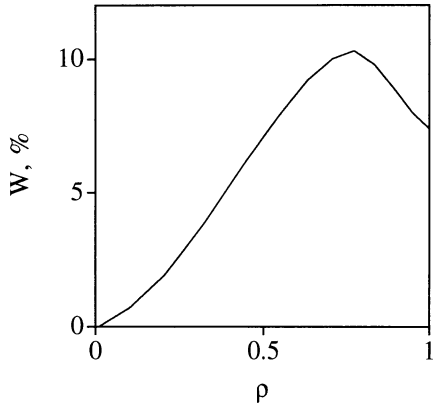

Figure 16. A magnetic well in an SHS with plasma current.

where

$$\varepsilon_{\mathrm{T}} = \sum_{m\neq 0} \varepsilon_{m_0} \cos(m\theta) \tag{6}$$

$$\varepsilon_{\mathrm{H}} = \left(\left(\sum_{m} \varepsilon_{mn_0} \cos(m\theta) \right)^2 + \left(\sum_{m} \varepsilon_{mn_0} \sin(m\theta) \right)^2 \right)^{1/2}. \tag{7}$$

To judge how good the configuration is optimized for transport, it is useful to compare the S-factor given by equation (5) with the factor S_0 calculated for the same configuration but including only definitely positive terms in the square brackets (so the cancellation caused by

the terms with different signs, or enhancement, in an unfavorable case, cannot be realized):

$$S_0 = \frac{1}{\rho^2}\int_0^{2\pi} \mathrm{d}\theta\, \varepsilon_{\mathrm{H}}^{3/2}\left[1.778\left(\frac{\partial \varepsilon_{\mathrm{T}}}{\partial \theta}\right)^2 + 0.684\left(\frac{\partial \varepsilon_{\mathrm{H}}}{\partial \theta}\right)^2\right]. \tag{8}$$

For the model field of equation (2), the ratio, S/S_0, can be written in the form

$$\frac{S}{S_0} = \frac{\int_0^{2\pi} \mathrm{d}\theta \sin^2\theta |1-\sigma\cos\theta|^{3/2}(1-1.2\sigma p + 0.385\sigma^2 p^2)}{\int_0^{2\pi} \mathrm{d}\theta \sin^2\theta |1-\sigma\cos\theta|^{3/2}(1+0.385\sigma^2 p^2)} \tag{9}$$

where $p = \varepsilon_{\mathrm{h}}/\varepsilon_{\mathrm{t}}$. The integrals in equation (9) can easily be computed and the results are presented in figures 17 and 18. Figure 17 shows contours of S/S_0 as function of σ and p, with full curves designating the contours with $S/S_0 \geqslant 1$, and dashed contours with $S/S_0 < 1$. The difference between neighbouring contours is 0.064. Location of the minimum, which is about 0.033, is shown by the bold dashed curves, while the location of the maximum ($\approx$1.97) is shown by the bold full curves. Figure 18 presents the same data but only for four different values of the parameter p: 1.5, 1, 0.5, and 0.25. The main conclusion that one can make from these figures is that in a situation, when the main helical harmonic is small (p is small), additional harmonics cannot improve or degrade the transport significantly. In an opposite situation with large p, however, additional harmonics have a dramatic effect on transport which can be improved significantly (for this model field by a factor of 30). On the other hand, improper choice of additional harmonics in this case can degrade the particle transport.

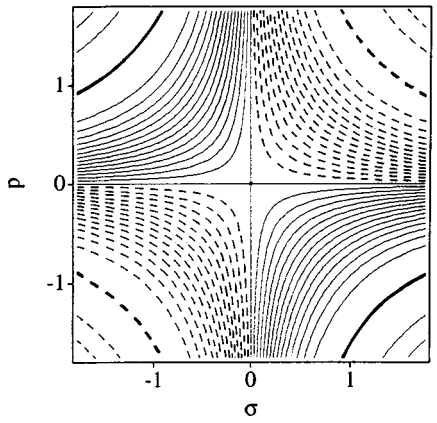

Figure 17. Contours of S/S_0 in the σ–p plane. Full contours correspond to $S/S_0 \geqslant 1$, and dashed contours to $S/S_0 < 1$. The difference between neighbouring contours is 0.064. The minimum of 0.033 is shown by the bold dashed curves.

The S-factor calculations for the SHS configurations of sections 3, 4, and 5 are presented in figure 19, where the radial dependence of S/S_0 is shown. One can see the reduction of the parameter S in comparison with S_0 up to a factor of five for the cases without plasma current and up to a factor of seven for the case with plasma current. This reflects the improvement of the collisionless particle transport. Further optimization of the SHS configuration by adjusting the currents in the coils or modifying the HCP winding law might, probably, improve this factor further and bring it closer to that discussed above for the model field (2) with optimized parameters.

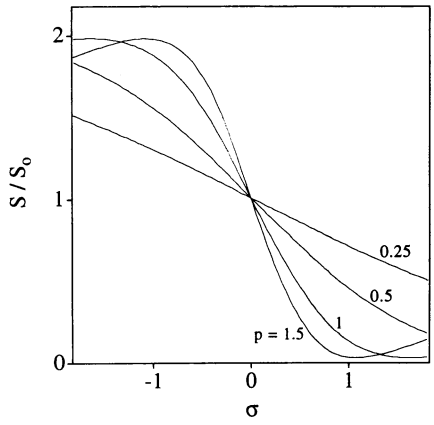

Figure 18. S/S_0 as a function of σ for four values of p.

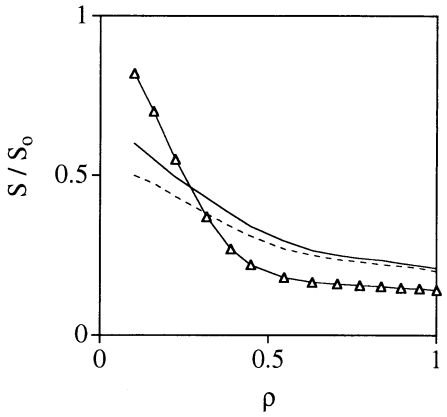

Figure 19. The radial dependence of S/S_0 for the SHS configuration without PF rings (full curve), with PF rings (dashed curve), and with plasma current (triangles).

The ratio S/S_0 in figure 19 shows the improvement in particle transport caused by the proper location of the helical ripple. This, however, is not a full description because the helical ripple can be large and might in principle cause significant ripple transport. The Monte Carlo transport simulations are thus of importance for a full evaluation of the neoclassical transport and for comparison with that in an equivalent tokamak (EQT). We define EQT as an axisymmetric device with the same rotational transform as a given stellarator and with the plasma major radius, minor radius, and elongation equal to the average corresponding quantities in a stellarator. The details of the methodics used in the Monte Carlo transport simulations and the results obtained will be presented in a separate publication. Here, we show just a few results for the diffusion coefficient, D_{i}, for ions (electron ripple transport is smaller), confirming good transport characteristics in the SHS configurations considered. No radial electric field is imposed (if present it can significantly improve the transport of thermal particles).

Particle transport in a stellarator depends significantly on the spectrum of the magnetic field harmonics, ε_{mn}, in equation (4). Corresponding calculations have been carried out for

all three SHS cases discussed above. For comparison, the Boozer harmonics, ε_{mn}, are shown in figures 20(a) and (b) for the case of the vacuum configuration of section 3 without PF rings (24 TF coils are considered, however) and for the case with plasma current of section 5. The ε_{mn} spectrum for the configuration of section 4 is close to that of figure 18(a) and is not shown. The strongest harmonics are labelled with (m, n) numbers. One can see that the toroidally symmetric harmonics with $n = 0$ are the strongest everywhere except at the very vicinity of the magnetic axis, where the mirror harmonic (0, 1) is the largest. Strong helical harmonics have $n = 1$, and harmonics with $n = 2$ have small amplitudes (<4% even near the plasma edge). All other harmonics are negligible.

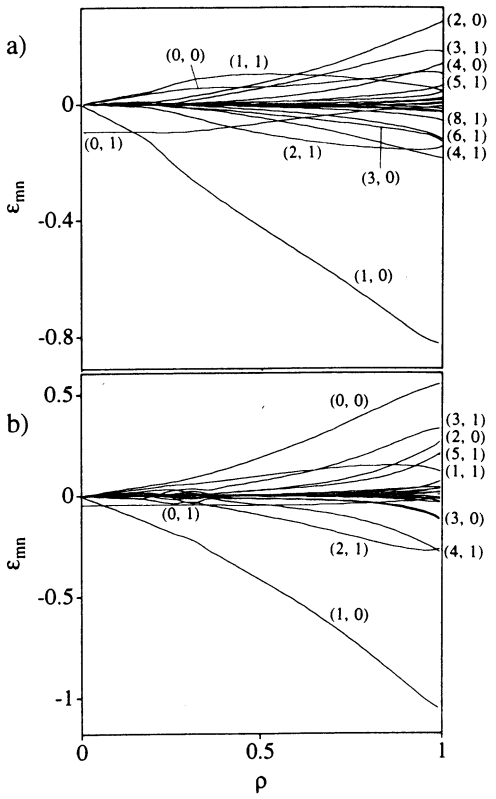

Figure 20. The magnetic field spectrum in an SHS without PF rings: (a) the vacuum configuration; (b) the configuration with plasma current.

According to theory, transition to the low collisionality ripple regime occurs at $\nu^*_{\rm st} < 1$, where

$$\nu^*_{\rm st} = \nu/(\varepsilon_{\rm h}^{\rm eff})^{3/2}\omega_{\rm b} \tag{10}$$

while ν is the total collision frequency of a test particle, ω_b is the bounce frequency,

$$\omega_{\rm b} = \frac{V|n_0 - m_0\iota|}{R} \tag{11}$$

and the effective helical ripple for the case of multiple harmonics can be calculated as

$$\varepsilon_{\rm h}^{\rm eff} = \frac{\pi}{2}\left\langle \left| \sum_{n\neq 0} \varepsilon_{mn} \cos(m\theta - nN\varphi) \right| \right\rangle. \tag{12}$$

In equation (11), $V = \sqrt{2E/M}$ is the velocity of a test particle with mass M, and n_0 and m_0 correspond to the main helical harmonic at a given flux surface. In equation (12), the angle brackets denote averaging over θ and φ. The values of ε_h^{eff} at $\rho = 0.5$ for all three SHS configurations considered are the following: $\varepsilon_h^{eff} = 0.128$ for the vacuum configuration without PF rings, 0.174 for the vacuum configuration with PF rings, and 0.11 for the configuration with the plasma current.

In figure 21 we present the results of Monte Carlo simulations for the ion diffusion coefficients D_i (calculated for a hydrogen plasma at $\rho = 0.5$ for $B_0 = 1$ T, a kinetic energy of test protons of $E_h = 300$ eV, and background plasma temperature $T_e = T_i = 300$ eV) in the wide range of the collisionality parameter ν_{st}^* for all three SHS configurations discussed.

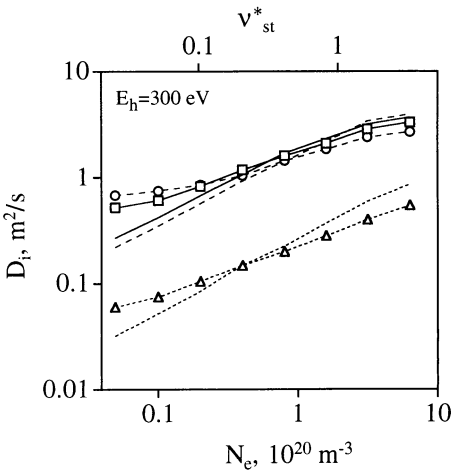

Figure 21. D_i in the SHS calculated for a vacuum configuration without PF rings (full curve with squares), for a vacuum configuration with PF rings (dashed curve with circles), and for a configuration with plasma current (dotted curve with triangles). The results for the corresponding EQTs are shown by the same types of curves but without the symbols.

Comparisons with that for the corresponding EQTs are also shown. For demonstration purposes, the values of ν_{st}^* for the case of the vacuum configuration without PF rings are also shown on the top horizontal axis of figure 21. As one can see, D_i in the SHS and the corresponding EQT is approximately the same for all SHS configurations. Also, it is important to notice that our transport simulations for the SHS do not indicate the $D_i \sim 1/\nu$ regime of poor low-collisional particle confinement, typical for a standard stellarator. In the SHS considered, D_i is a monotonically decreasing function for lower collisionality, which is very advantageous for fusion reactor applications. This agrees with the optimization effect of the inboard location of the helical ripple, stressed by the S-factor reduction in figure 19. It is important to notice also that the diffusion drops significantly for the case with plasma current (the curve marked by triangle symbols). This is another indication of the importance of having a positive plasma current in SS-type configurations.

7. Discussion and conclusions

A novel stellarator concept, the helical post stellarator (HPS), has been proposed. The calculations have been presented for a particular HPS, the single-helix stellarator (SHS). This

configuration has a number of features which are unique and very unusual in comparison with those of traditional stellarators. Thus, the SHS holds a few records for stellarators.

The unique feature of the SHS is that the only helical element of its coil system is the helical centre post, which produces stellarator magnetic fields with the magnetic ripple located inboard, while the outboard parts of the coils are similar to those in a toroidally symmetric device such as a tokamak. Theoretically, it was shown [35, 36] that this type of harmonic composition can lead to efficient collisionless plasma confinement. Our calculations of the S-factor and Monte Carlo simulations for the SHS confirmed this conclusion.

To our knowledge, the SHS is the only high rotational transform configuration with compact coils having just a single toroidal period (although two other $N = 1$ stellarator configurations were proposed in the past, the Cleftron [33] and the Ultra-Simple Stellarator [34]). The plasma aspect ratio, $A \approx 1$, is also out of the range ever considered for stellarators. The SHS features the most compact and the most spherical plasma among all SS configurations previously discussed, and thus can be considered as a new member of the spherical stellarator family.

The SHS coil system is efficient for producing strong magnetic fields in the plasma region with moderate currents in the coils. Effective control over the plasma location, magnetic field magnitude, and magnetic ripple can be accomplished by a system of PF rings with very moderate currents, although the configuration of interest can be obtained even without PF rings.

The vacuum rotational transform produced in the SHS is rather high for such extremely low aspect ratios and reaches values of 0.12–0.15. Also, the rotational transform is a decreasing function of minor radius, similar to that in an ST with ohmic current, or to that in the SS configurations considered before [15–22]. This is convenient for adding the plasma current to the system and for avoiding resonant harmonics which otherwise might lead to magnetic islands. No significant magnetic island structure was found for the vacuum SHS configurations considered.

Three different SHS configurations have been analysed in this paper: an SHS without PF rings ($A = 1.17$), an SHS with PF rings ($A = 1.02$), and an SHS with plasma current ($A = 1.25$). For all three configurations considered, it has been shown that the particle transport is as good as that in equivalent tokamaks for a wide range of the collisionality parameter, ν^*_{st}. Two important effects of the plasma current have been demonstrated: producing a magnetic well (important for MHD stability) and improving particle transport.

One more advantage of the HPS is the simplicity of the coil system, with the HCP being the major technological element. The HPS can be easily built from the corresponding ST by replacing the straight centre post with the HCP or by winding a helix around the straight centre post of an ST. For a reactor, if necessary, the HCP can be made removable, as it is proposed for a centre post in an ST [14]. To eliminate the outboard magnetic ripple, which might be dangerous for particle transport, the large number or remote location of the return limbs of the TF coils can be used. For any real device, this would need to be optimized taking into account requirements for plasma access, heating and diagnostics, capital cost, and electricity consumption.

The HPS has the potential to resolve a few problems of the ST approach. One of them is steady-state operation which is problematic for an ST but is natural for an HPS as it is a stellarator device. Another severe problem of an ST reactor is the strong heat flux to the centre post from the plasma which is practically in direct contact with the centre post structure. In contrast, the plasma in the HPS is separated from the HCP by the divertor region from where the energetic particles leaving the plasma can be removed before they

reach the HCP. These particles follow the field lines to the top and bottom regions where the toroidally symmetric divertor plates can be conveniently installed.

This paper introduces the SHS configuration and presents the first results for its magnetic field structure and properties in the case of very low plasma pressure. For fusion applications, however, the most important regimes of operation are the high-β regimes. We are planning to address the corresponding issues in future publications. At the present time, one can only suggest that the stability limits for the SHS will be very high and close to those in an ST. The basis for such suggestions can be the fact that the most dangerous MHD modes, which, in principle, can be unstable at high β, grow on the outboard of the torus where an SHS configuration features toroidal symmetry and is very similar to an ST.

Many engineering details, including the generated forces and a necessary supporting structure for the HCP, should be clarified before an actual SHS can be built. We believe that the HCP can be optimized to significantly reduce the $\boldsymbol{J} \times \boldsymbol{B}$ forces (in comparison with that for a centre post in an ST) by reducing the angle between the vectors of the current density, $\boldsymbol{J}$, in the HCP and the local magnetic field, $\boldsymbol{B}$. A simple supporting structure for an HCP can be built, for example, as a reinforced straight column located along the Z-axis (without any current; or with some relatively small current in case one would like to have better control over the rotational transform).

While this paper was under review, a few new results were obtained for the HPS and a few relevant presentations [44–48] were made, which we would like to mention here. The most important new results of these presentations were: (1) consideration of the double-helix stellarator (DHS) and triple-helix stellarator (THS) configurations featuring the centre posts consisting, respectively, of two and three helices; (2) demonstration of the strong and positive effects of the plasma current in a DHS on the characteristics of the high-β MHD equilibria and particle transport; and (3) calculation of the bootstrap current in a DHS and demonstration of the extremely high-β MHD equilibria ($\beta_0 = 86\%$, $\beta = 20\%$) accessible with the bootstrap current alone.

Acknowledgments

In conclusion, the author is thankful to S P Hirshman for permission to use the 3D MHD equilibrium code, VMEC. He would also like to acknowledge useful discussions of various related questions with S P Hirshman, D B Batchelor, D A Spong, J D Callen and D A Monticello. This work was partially supported by the US DOE grant No DE-FG02-97ER54395.

References

[1] Lyon J F, Carreras B A, Lynch V E *et al* 1989 *Fusion Technol.* **15** 1401
[2] Okamura S, Matsuoka K, Nishimura K *et al* 1995 *Nucl. Fusion* **35** 283
[3] Knowlton S F, Gandy R F *et al* 1993 *J. Fusion Energy* **12** 261
[4] Blackwell B D, Borg G G, Dewar R L *et al* 1995 *Proc. 15th Int. Conf. on Plasma Phys. and Contr. Nucl. Fusion Res. (Seville, 1994)* vol 2 (Vienna: International Atomic Energy Agency) p 337
[5] Geiger J, Goermer C, Hofmann J V *et al* 1997 *Stellarator News* **53** 3
[6] Wakatani M and Sudo S 1996 *Plasma Phys. Control Fusion* **38** 937
[7] Sykes A 1994 *Plasma Phys. Control Fusion* **36** B93
[8] Ono M *et al* 1993 *Proc. Int. Conf. on Plasma Phys. and Contr. Fusion Res. (Wurzburg 1992)* vol 1 (Vienna: International Atomic Energy Agency) p 693
[9] Martin A K and Jarboe T R 1996 *Plasma Phys. Control Fusion* **38** 1967
[10] Golant V E *et al* 1997 *Proc. 16th Int. Conf. on Plasma Phys. and Contr. Nucl. Fusion Res. (Montreal, 1996)* vol 3 (Vienna: IAEA) p 591

[11] Fonck R *et al* 1996 *Bull. Am. Phys. Soc.* **41** 1400
[12] Todd T N, Bond A, O'Brien M *et al* 1997 *IAEA Tech. Committee Meeting 'Innovative Approaches to Fusion Energy' (Pleasanton, CA, October 20–23, 1997)* IAEA-LLNL
[13] Peng Y-K M, Colchin R J, Hedrick C L *et al* 1995 *Proc. 15th Int. Conf. of Plasma Phys. and Contr. Fusion Res. (Seville, 1994)* vol 2 (Vienna: International Atomic Energy Agency) p 643
[14] Sviatoslavsky I N, Mogahed E A, Peng Y-K M *et al* 1996 *Fusion Technol.* **30** 1649
[15] Moroz P E 1996 *Phys. Rev. Lett.* **77** 651
[16] Moroz P E 1996 *Phys. Plasmas* **3** 3055
[17] Moroz P E 1997 *Plasma Phys. Rep.* **23** 502
[18] Moroz P E 1997 *Plasma Phys. Control. Fusion* **39** 1841
[19] Moroz P E 1997 *Nucl. Fusion* **37** 1045
[20] Moroz P E 1996 *Stellarator News* **48** 2
[21] Moroz P E, Batchelor D B *et al* 1996 *Fusion Technol.* **30** 1347
[22] Moroz P E, Batchelor D B *et al* 1996 *Bull. Am. Phys. Soc.* **41** 1567
[23] Batchelor D B, Carreras B A, Hirshman S P *et al* 1996 *Bull. Am. Phys. Soc.* **41** 1568
[24] Spong D A, Hirshman S P and Whitson J C 1997 *Plasma Phys. Rep.* **23** 483
[25] Spong D A, Hirshman D P and Whitson J C 1997 *Stellarator News* **52** 1
[26] Ross D W, Valanju P M, He H *et al* 1997 *Plasma Phys. Rep.* **23** 492
[27] Garabedian P R 1996 *Phys. Plasmas* **3** 2483
[28] Garabedian P R 1997 *Phys. Plasmas* **4** 1617
[29] Garabedian P R 1997 *Plasma Phys. Control. Fusion* **39** B129
[30] Reiman A *et al* 1997 *Bull. Am. Phys. Soc.* **42** 1913
[31] Zarnstorff M C *et al* 1997 *Bull. Am. Phys. Soc.* **42** 1914
[32] Goldston R J 1997 *IAEA Tech. Committee Meeting 'Innovative Approaches to Fusion Energy' (Pleasanton, CA, October 20–23, 1997)* IAEA-LLNL
[33] Ohkawa T 1981 *Proc. 3rd Stellarator Workshop (Moscow, 1981)* p 111
[34] Todd T N 1990 *Plasma Phys. Control. Fusion* **32** 459
[35] Mynick H E, Chu T K and Boozer A H 1982 *Phys. Rev. Lett.* **48** 322
[36] Shaing K C and Hokin S A 1983 *Phys. Fluids* **26** 2136
[37] Galeev A A, Sagdeev R Z, Furth H P and Rosenbluth M N 1969 *Phys. Rev. Lett.* **22** 511
[38] Connor J W and Hastie R J 1974 *Phys. Fluids* **17** 114
[39] Potok R E, Politzer P A and Lidsky L M 1980 *Phys. Rev. Lett.* **45** 1328
[40] Bykov V E, Georgievskij A V *et al* 1984 *Nucl. Fusion* **24** 1195
[41] Moroz P E 1995 *Phys. Plasmas* **2** 4269
[42] Hirshman S P, Rij W I and Merkel P 1986 *Comput. Phys. Commun.* **43** 143
[43] Boozer A H 1982 *Phys. Fluids* **25** 520
[44] Moroz P E 1997 Double-helix stellarator *UW-Madison Report* UW-CPTC 97-16 *Nucl. Fusion* accepted for publication
[45] Moroz P E 1997 *IAEA Tech. Committee Meeting 'Innovative Approaches to Fusion Energy' (Pleasanton, CA, October 20–23, 1997)* IAEA-LLNL
[46] Moroz P E 1997 *Stellarator News* **54** 6
[47] Moroz P E 1997 *Bull. Am. Phys. Soc.* **42** 1914
[48] Moroz P E 1997 *Bull. Am. Phys. Soc.* **42** 2070